Science Advances

AAAS

advances.sciencemag.org/cgi/content/full/2/6/e1501624/DC1

Supplementary Materials for

A highly shape-adaptive, stretchable design based on conductive liquid for energy harvesting and self-powered biomechanical monitoring

Fang Yi, Xiaofeng Wang, Simiao Niu, Shengming Li, Yajiang Yin, Keren Dai, Guangjie Zhang, Long Lin, Zhen Wen, Hengyu Guo, Jie Wang, Min-Hsin Yeh, Yunlong Zi, Qingliang Liao, Zheng You, Yue Zhang, Zhong Lin Wang

Published 17 June 2016, *Sci. Adv.* **2**, e1501624 (2016)
DOI: 10.1126/sciadv.1501624

This PDF file includes:

- fig. S8. Simulation results showing the increasing electrical potential difference between the two electrodes for saTENG units working in the attached-electrode sliding mode and freestanding mode.
- fig. S9. Increasing conductivity of the NaCl solution with the increasing weight concentration.
- fig. S10. Experimental setup for the stretchability test.
- fig. S11. Cycle test of the saTENG under the original state.
- fig. S12. Cycle test of the saTENG under the stretched state.
- fig. S13. Equivalent circuit diagrams for the LED arrays in demonstrations.
- fig. S14. Demonstrations of the sliding-mode and freestanding-mode saTENGs to harvest energy from human motion.
- Legends for movies S1 to S11

Other Supplementary Material for this manuscript includes the following:
(available at advances.sciencemag.org/cgi/content/full/2/6/e1501624/DC1)

- movie S1 (.mov format). Harvesting energy from foot motion by an outsole saTENG.
- movie S2 (.mov format). A bracelet-like saTENG worn on a human wrist to harvest energy from tapping motion.
- movie S3 (.mov format). Charging an aluminum electrolytic capacitor by a bracelet-like saTENG.
- movie S4 (.mov format). A bracelet-like saTENG worn on the upper arm to monitor arm motion.
- movie S5 (.mov format). Harvesting energy by a large-area cushion-like saTENG tapped by an acrylic plate.
- movie S6 (.mov format). Harvesting energy by a large-area cushion-like saTENG touched by human skin.
- movie S7 (.mov format). Harvesting mechanical energy based on household plumbing, using flowing water as the electrode.
- movie S8 (.mov format). Harvesting energy from arm swing by a saTENG working in the single-electrode sliding mode.
- movie S9 (.mov format). Harvesting energy from arm motion by an attached-electrode-mode saTENG.
- movie S10 (.mov format). Harvesting energy from moving a mouse by a freestanding-mode saTENG.
- movie S11 (.mov format). Harvesting energy from human walking by a freestanding-mode saTENG.

note S1. Detailed information for the simulation modeling.

The geometry for each simulation is drawn by the COMSOL software. A 2D model was utilized to simplify the calculation. Owing to the triboelectric effect, when the nylon (or aluminum) and the rubber are separated after contact, the nylon surface (or aluminum surface) and the top surface of the rubber will have charges with different signs. The nature of the triboelectric effect makes it reasonable to assume that the generated triboelectric charges are uniformly distributed on these two surfaces, which is an excellent approximation for insulators. Also, the decay of triboelectric charges with time can be neglected since the insulators have the ability to maintain their triboelectric charges for a long time (1). Due to the charge conservation, the nylon surface (or aluminum surface) and the rubber's top surface have the same amount of triboelectric charges; so the triboelectric charge density can be calculated. The overall density for the triboelectric charges on the overlapped surface can be regarded as the summation of the charge density on each surface. The entire structure is surrounded by air, which is the same as the usual case in experiments. The potential at infinity is chosen as the reference point for the electric potential, which is 0. The material property is also assigned in the COMSOL software. Subsequently, the required electrostatic properties can be calculated by utilizing the COMSOL software electrostatics module. Detailed calculation procedure can be referred to References (2), (3), (4) and (5).

Parameters for the established models (these parameters will affect only the magnitude of but not the changing trend of the calculated results):

(1) Figure 2E: the triboelectric charge density on the nylon surface was assigned to be 10 $\mu C/m^{-2}$; the thickness and length of the nylon were set to be 100 μm and 50 mm; the thickness and length of the aluminum film deposited on the nylon's top surface were set to be 100 μm and 50 mm; the thickness and perimeter of the rubber were set to be 200 μm and 40 mm; the interval between the nylon and the top

point of the rubber in the final state was set to be 50 mm. The width of the structure was set to be 100 mm.

(2) Figure S8: the triboelectric charge density on the aluminum surface was assigned to be 10 μC/m^{-2}; the thickness and length of the aluminum were set to be 50 μm and 50 mm; the diameter (height) and the length of the rubber were set to be 12.7 mm and 50 mm; the interval between the two shape-adaptive triboelectric nanogenerator (saTENG) units for fig. S8B was set to be 10 mm. The width of the structure for fig. S8A and fig. S8B were both set to be 100 mm.

(3) Figure S6: the triboelectric charge density on the nylon surface was assigned to be 10 μC/m^{-2}; the thickness and length of the nylon were set to be 100 μm and 50 mm; the perimeter of the rubber was set to be 40 mm; the interval between the nylon and the top point of the rubber in the final state was set to be 0 mm. A reference electrode was put under the liquid electrode to serve as the ground, which had a length of 50 mm, a thickness of 100 μm, and was 30 mm away from the center of the liquid electrode. The width of the structure was set to be 100 mm.

Note that for simplification, the acrylic plate support under the saTENG unit is omitted in the simulation model, which will not affect the changing trend of the electrical potential due to the superposition principle of electrical potential.

note S2. Factors affecting TENG's inherent impedance.

TENG is based on the electrostatic induction and has inherent capacitive behavior. Its intrinsic impedance can be estimated to be:

$$\mathbf{Z} = \frac{\mathbf{1}}{\mathbf{2}\boldsymbol{\pi} \boldsymbol{f} \boldsymbol{C}} \tag{S1}$$

where f is the frequency of the external motion, C is the inherent capacitance between the single electrode and the ground for the single-electrode-mode TENG or the average capacitance between the two electrodes for the attached-electrode-mode TENG. For a rationally designed TENG, the two

electrodes are fully-insulated and the internal resistance is nearly infinity. Since TENG's inherent capacitance is generally in the order of tens or hundreds of pF; if the external motion has a low frequency (about 0.4 to 4 Hz in the experiments), the intrinsic impedance of the TENG will be very high (in the range of hundreds of MΩ). Generally, the inherent impedance of the single-electrode-mode TENG is higher than that of the attached-electrode-mode TENG since the inherent capacitance of the single-electrode-mode TENG is usually lower due to the larger distance between the single electrode and the ground.

note S3. Consequences of the saTENG's high inherent impedance.

For a TENG that has a negligible electrode resistance, when it is connected to a resistive load, the equivalent circuit model can be shown as:

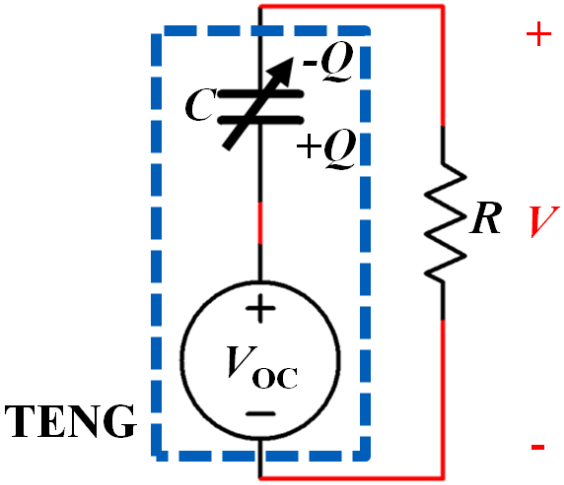

If we consider the effect of the TENG's electrode resistance, the equivalent circuit model now adds a new term, which is the electrode resistance r.

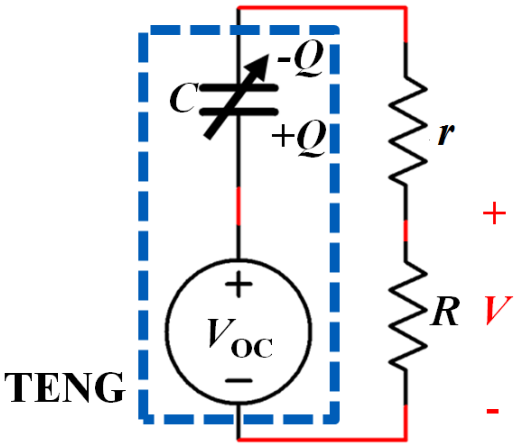

The power applied to the external resistance R can be estimated by: (For simplification, the V_{oc} is assumed as a sinusoidal profile in the analysis.)

$$P = \frac{{V_{OC}}^2 R}{\frac{1}{\omega^2 C^2} + (r+R)^2} \tag{S2}$$

It is clearly shown from the above equation that when r is smaller than 1/100 ωC, the influence of r on P is very small. Since TENG's inherent impedance is generally in the range of hundreds of MΩ, the performance of the TENG will change very slightly as long as the TENG's electrode resistance is smaller than the MΩ range.

Another advantage that the TENG's high inherent impedance provides is that the voltage across the electrode will be small. The voltage across the electrode can be given as

$$\mathrm{V_{electrode}} = \frac{V_{OC} r}{\sqrt{\frac{1}{\omega^2 C^2} + (r+R)^2}} \tag{S3}$$

It can be seen that when r is smaller than 1/100 ωC (much smaller than the TENG's inherent impedance), the voltage across the electrode will be less than $0.01V_{oc}$, which is smaller than the electrolysis voltage of the conductive liquid.

note S4. Detailed explanation for the increasing contact area with the increasing elongation of the saTENG.

The cross-sectional area of the saTENG is assumed to remain unchanged under deformation, therefore

$$w_x(D - d_0) + \frac{\pi(D-d_0)^2}{4} = \frac{\pi D^2}{4} \tag{S4}$$

Let $(D - d_0)$ = y, then

$$w_x y + \frac{\pi y^2}{4} = \frac{\pi(y+d_0)^2}{4} \tag{S5}$$

Solve equation (S5) for w_x, we get

$$w_x = \frac{\pi {d_0}^2}{4y} + \frac{\pi d_0}{2} \tag{S6}$$

Since D reduces with the elongation and d_0 is the same at different stretched states, y decreases with the elongation. Thus w_x increases with the elongation of the saTENG.

The contact area between the nylon and the rubber is estimated to be

$$S = w_x L_0(1+\varepsilon) \tag{S7}$$

which also increases with the elongation of the saTENG.

note S5. Detailed derivation of Eq. 3. (The increasing resistance of the liquid electrode with the increasing elongation.)

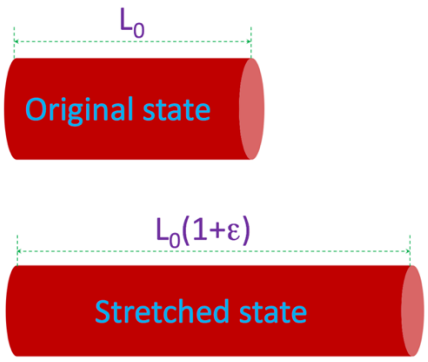

The resistance of the liquid electrode at the original state is

$$R_0 = \frac{L_0}{\sigma A_0} \tag{S8}$$

where is L_0 is the length of, A_0 is the cross-sectional area of, and σ is the electrical conductivity of the liquid electrode at the original state, respectively.

The length of the liquid electrode at the stretched state is

$$L_S = L_0(1+\varepsilon) \tag{S9}$$

Since the volume of the liquid electrode at the stretched state is the same as the original state, we have

$$A_s L_0(1+\varepsilon) = A_0 L_0 \tag{S10}$$

where A_s is the cross-sectional area of the liquid electrode at the stretched state.

Solve equation (S10) for A_s, we get

$$A_s = \frac{A_0}{(1+\varepsilon)} \tag{S11}$$

Thus the resistance of the liquid electrode at the stretched state is estimated to be

$$R_s = \frac{L_0(1+\varepsilon)}{\sigma\frac{A_0}{(1+\varepsilon)}} = \frac{L_0(1+\varepsilon)^2}{\sigma A_0} \tag{S12}$$

References

1. F. Saurenbach, D. Wollmann, B. D. Terris & A. F. Diaz. Force microscopy of ion-containing polymer surfaces: morphology and charge structure. *Langmuir : the ACS journal of surfaces and colloids* **8**, 1199-1203, (1992).
2. S. Niu, Y. Liu, S. Wang, L. Lin, Y. S. Zhou, Y. Hu & Z. L. Wang. Theoretical Investigation and Structural Optimization of Single-Electrode Triboelectric Nanogenerators. *Advanced Functional Materials* **24**, 3332-3340, (2014).
3. S. Niu, S. Wang, L. Lin, Y. Liu, Y. S. Zhou, Y. Hu & Z. L. Wang. Theoretical study of contact-mode triboelectric nanogenerators as an effective power source. *Energy & Environmental Science* **6**, 3576-3583, (2013).
4. S. Niu, Y. Liu, X. Chen, S. Wang, Y. S. Zhou, L. Lin, Y. Xie & Z. L. Wang. Theory of freestanding triboelectric-layer-based nanogenerators. *Nano Energy* **12**, 760-774, (2015).
5. S. Niu & Z. L. Wang. Theoretical systems of triboelectric nanogenerators. *Nano Energy* **14**, 161-192, (2015).

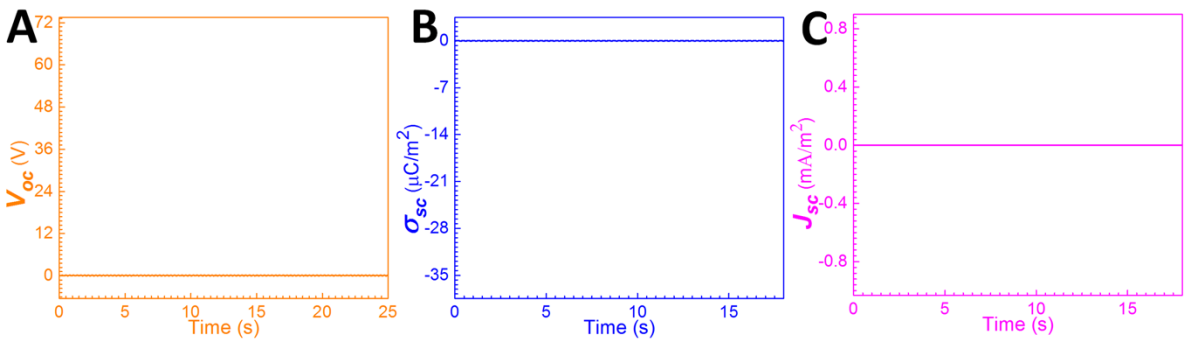

fig. S1. (A-C) The measured typical electrical responses of the saTENG unit with paraffin oil as the electrode (resistance >200 GΩ): (A) the open-circuit voltage (V_{oc}); (B) the short-circuit charge density (σ_{sc}); (C) the short-circuit current density (J_{sc}).

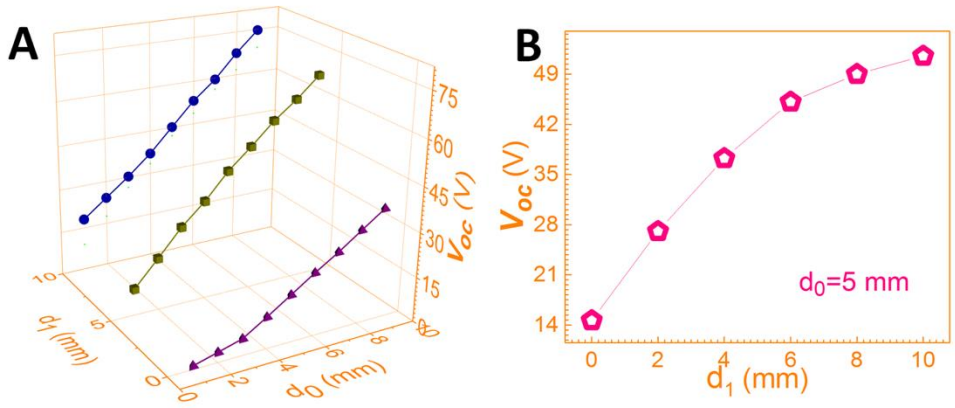

fig. S2. (A) Dependence of the open-circuit voltage (V_{oc}) on the deformation of the saTENG unit. (B) Dependence of the V_{oc} on the interval between the nylon and the rubber when the deformation degree of the saTENG is the same.

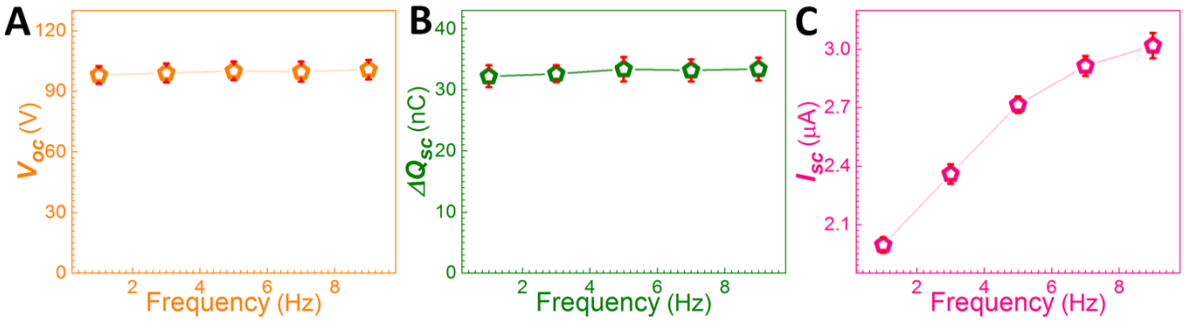

fig. S3. (A-C) Influence of the contact frequency of the two triboelectric surfaces on (A) the open-circuit voltage (V_{oc}), (B) the amount of the short-circuit transferred charge (ΔQ_{sc}), and (C) the short-circuit current (I_{sc}) of the single-electrode-mode saTENG.

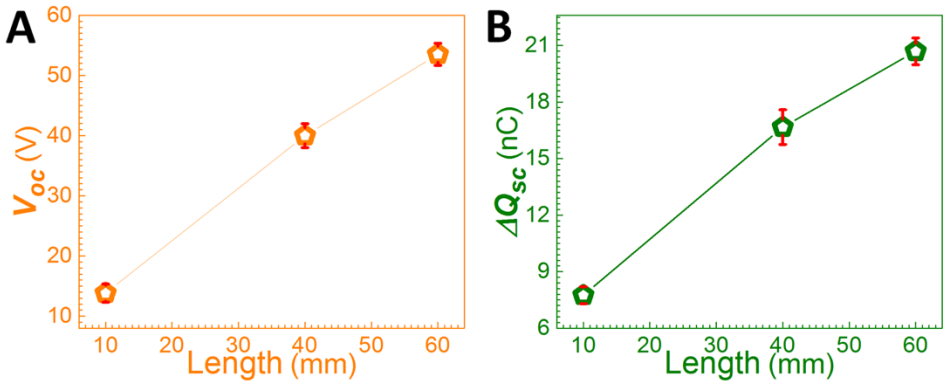

fig. S4. (A-B) Influence of the length of the saTENG unit on (A) the open-circuit voltage (V_{oc}) and (B) the amount of the short-circuit transferred charge (ΔQ_{sc}) of the single-electrode-mode saTENG.

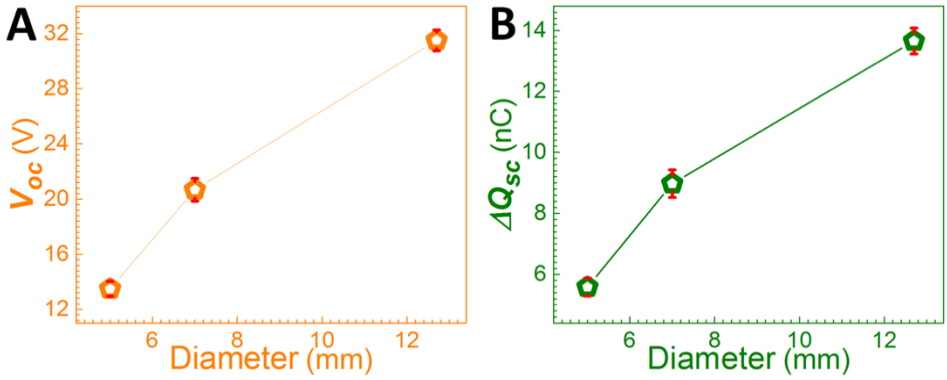

fig. S5. (A-B) Influence of the diameter of the saTENG unit on (A) the open-circuit voltage (V_{oc}) and (B) the amount of the short-circuit transferred charge (ΔQ_{sc}) of the single-electrode-mode saTENG.

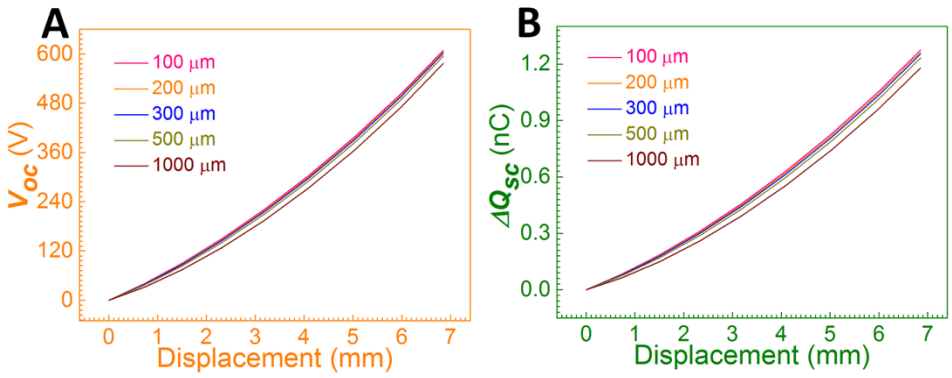

fig. S6. (A-B) Theoretical results of the influence of the thickness of the rubber cover on (A) the open-circuit voltage (V_{oc}) and (B) the amount of the short-circuit transferred charge (ΔQ_{sc}) of the single-electrode-mode saTENG.

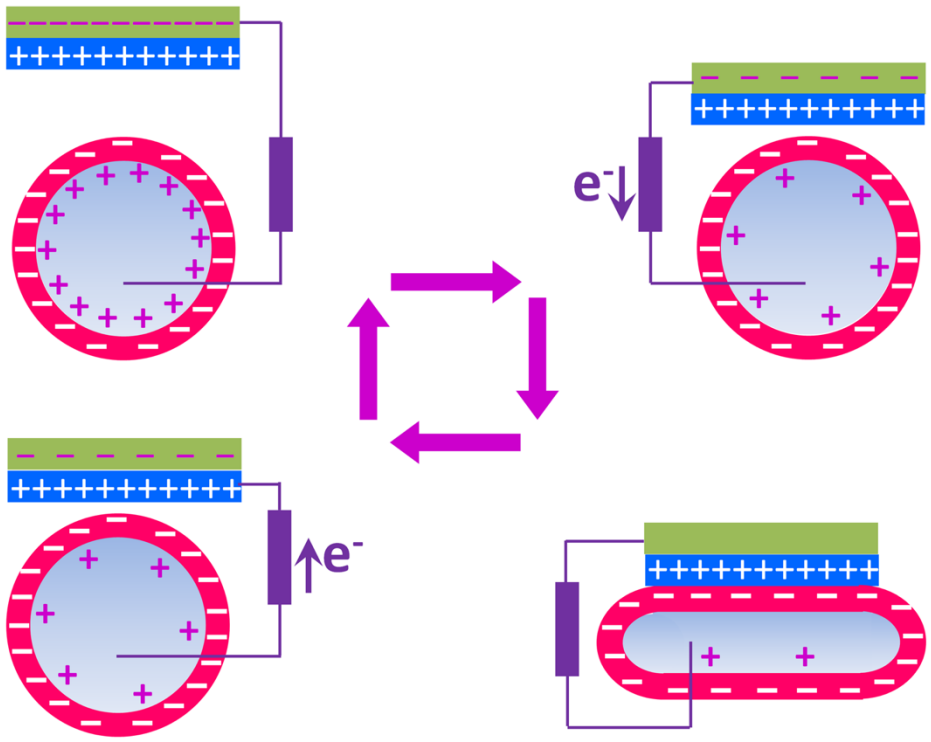

fig. S7. Schematic diagram exhibiting the operating mechanism for the saTENG working in the attached-electrode contact mode: the electric potential difference between the two electrodes decreases when the nylon approaches the rubber and then increases as the nylon departs from the rubber in the open-circuit condition, which drives electrons to flow back and forth between the two electrodes through the external load.

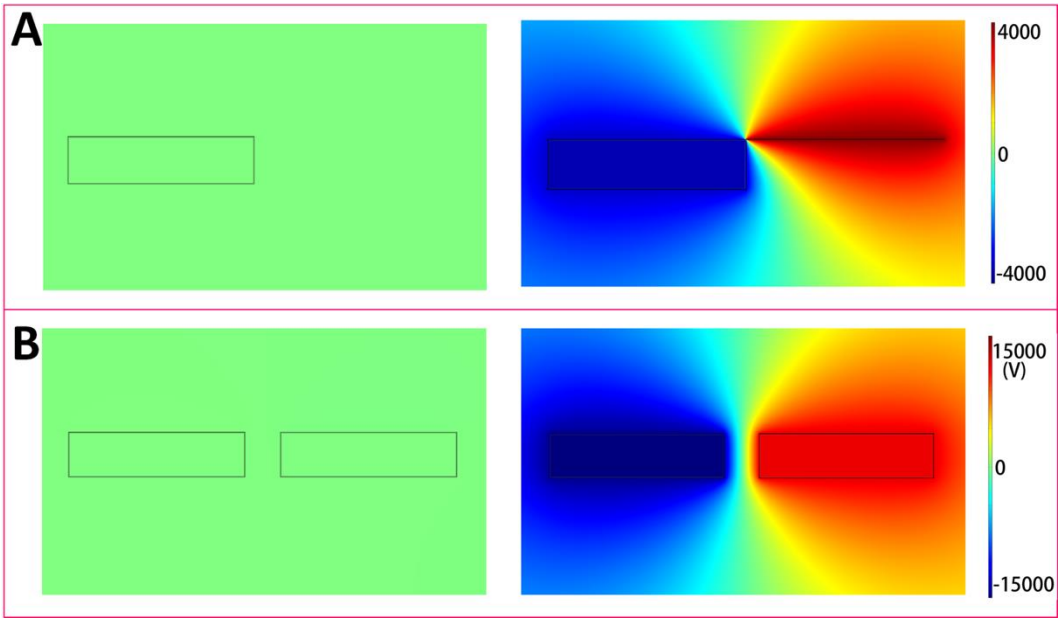

fig. S8. Simulation results showing the increasing electrical potential difference between the two electrodes for saTENG units working in (A) the attached-electrode sliding mode and (B) the freestanding mode.

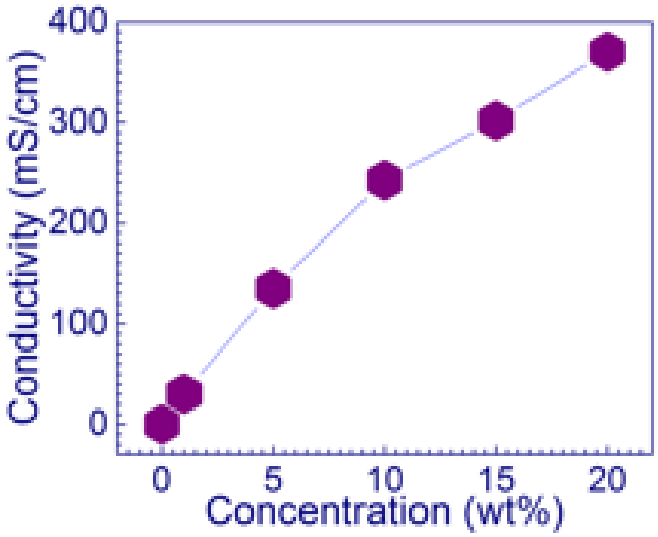

fig. S9. Increasing conductivity of the NaCl solution with the increasing weight concentration.

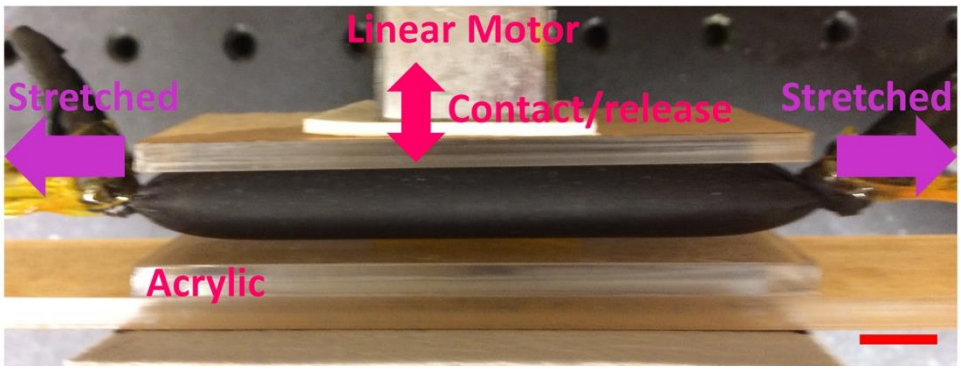

fig. S10. Experimental setup for the stretchability test. Scale bar: 1cm.

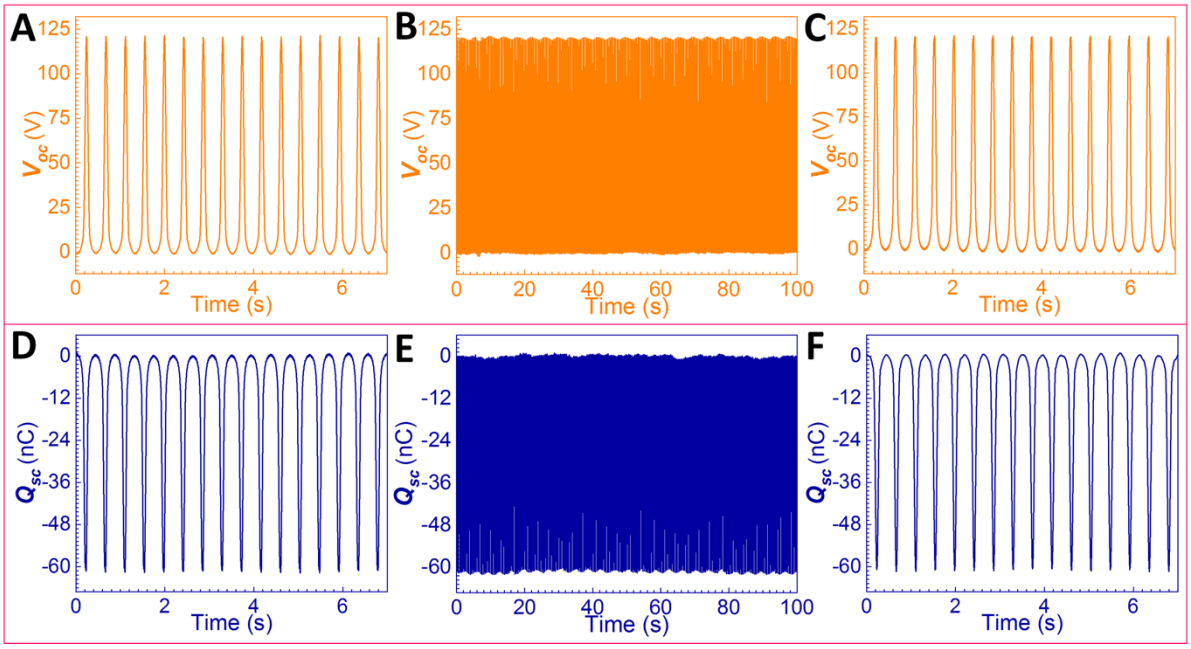

fig. S11. Cycle test of the unstretched saTENG: (A-C) the measured open-circuit voltage (V_{oc}) (A) before, (B) during and (C) after ~55,000 contact/release cycles between the acrylic and the rubber cover of the saTENG under the original state; (D-F) the measured short-circuit charge (Q_{sc}) (D) before, (E) during and (F) after ~55,000 contact/release cycles between the acrylic and the rubber cover of the saTENG under the original state.

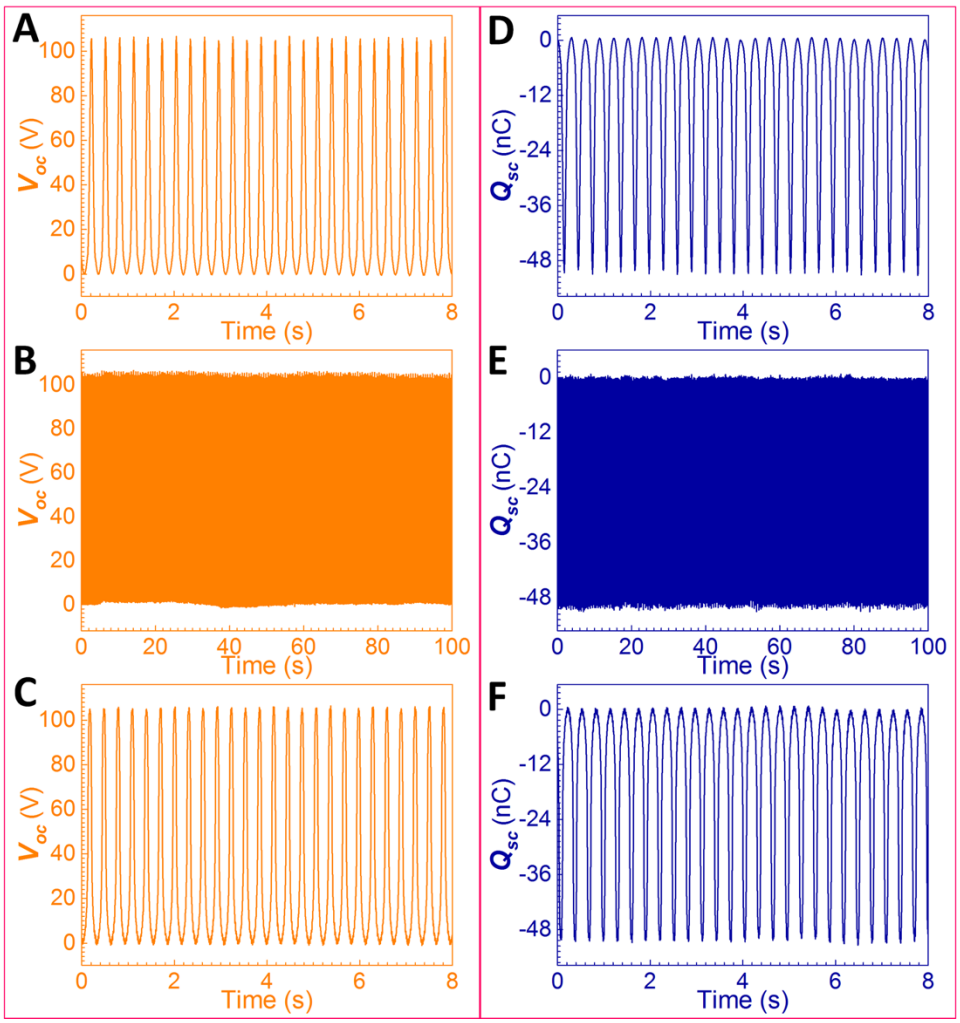

fig. S12. Cycle test of the stretched saTENG: (A-C) the measured open-circuit voltage (V_{oc}) (A) before, (B) during and (C) after ~55,000 contact/release cycles between the acrylic and the rubber cover of the saTENG under the stretched state (tensile strain: 300%); (D-F) the measured short-circuit charge (Q_{sc}) (D) before, (E) during and (F) after ~55,000 contact/release cycles between the acrylic and the rubber cover of the saTENG under the stretched state (tensile strain: 300%).

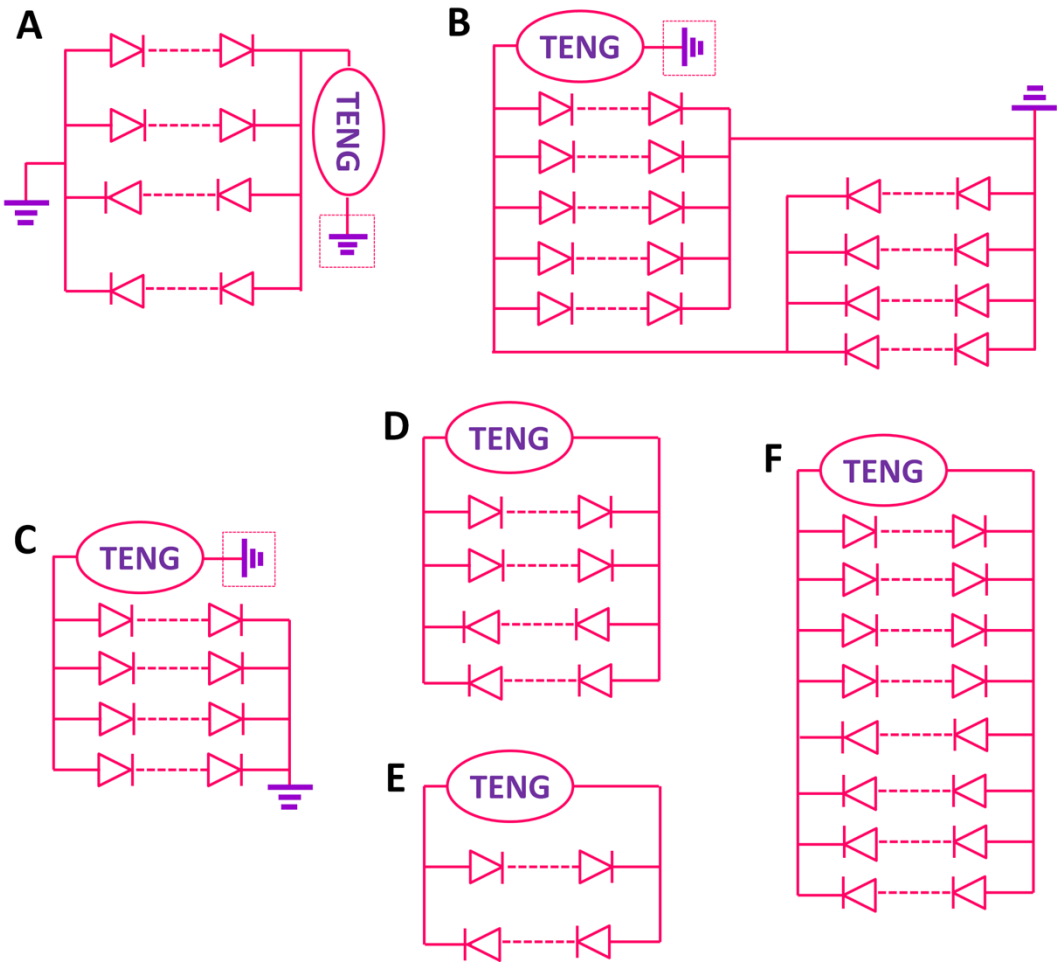

fig. S13. Equivalent circuit diagrams for the LED arrays in demonstrations shown in (A) Fig. 4D and fig. S14A; (B) Fig. 5A-B; (C) Fig. 5E-F; (D) fig. S14B; (E) fig. S14C; (F) fig. S14D.

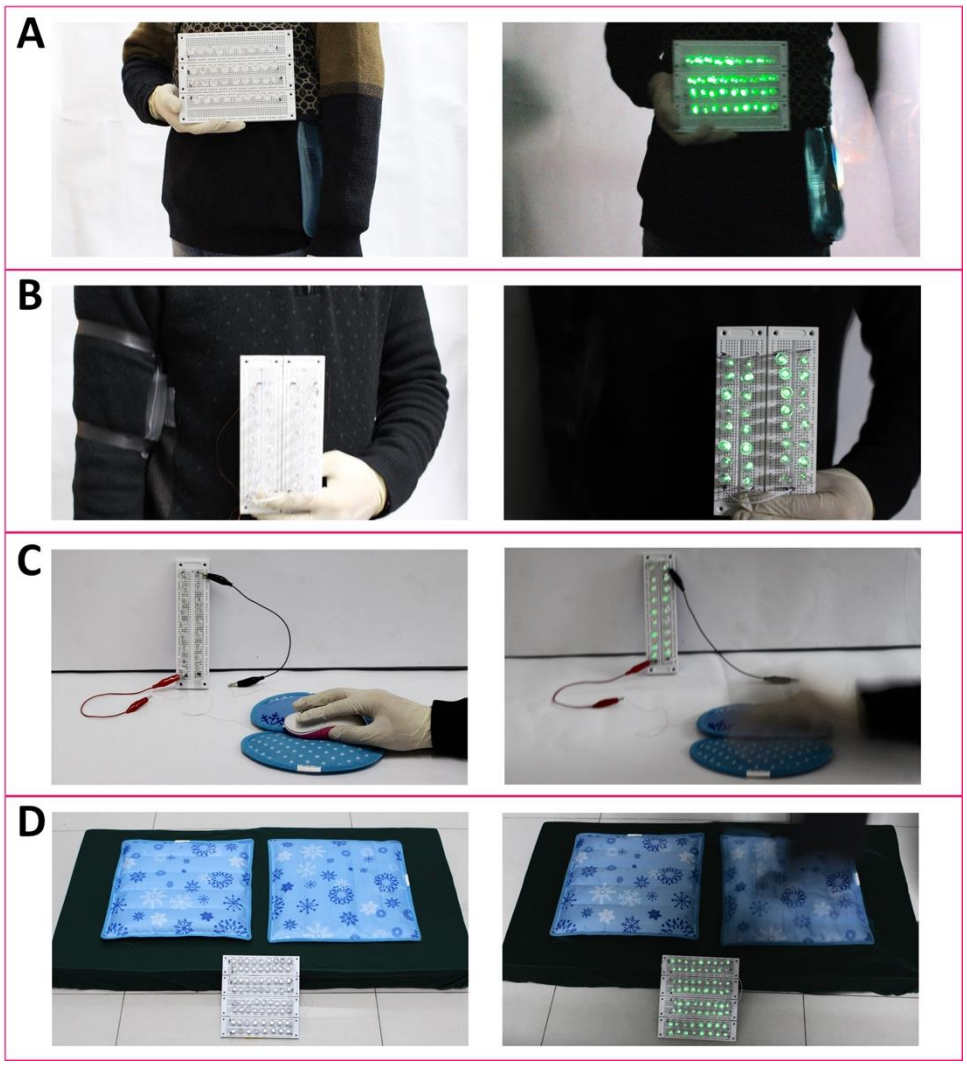

fig. S14. Demonstrations of the sliding-mode and freestanding-mode saTENGs to harvest energy from human motion. (A) Photographs showing a saTENG mounted on the side of the human torso to harvest energy from arm swing. The saTENG was working in the single-electrode sliding mode, with the human body served as the ground. (B) Photographs showing a saTENG working in the attached-electrode mode to harvest energy from arm motion. A pad-like saTENG unit was mounted on the upper arm; and a layer of PTFE film with copper film deposited on one surface was laminated on the human torso, with the PTFE surface facing the saTENG unit. The copper film served as the other electrode. (C) Photographs showing a saTENG working in the freestanding mode to harvest energy from moving the mouse. (D) Photographs showing a saTENG working in the freestanding mode to harvest energy from human walking.

Supplementary Movies

movie S1. Harvesting energy from foot motion by an outsole saTENG.

movie S2. A bracelet-like saTENG worn on a human wrist to harvest energy from tapping motion.

movie S3. Charging an aluminum electrolytic capacitor by a bracelet-like saTENG.

movie S4. A bracelet-like saTENG worn on the upper arm to monitor arm motion.

movie S5. Harvesting energy by a large-area cushion-like saTENG tapped by an acrylic plate.

movie S6. Harvesting energy by a large-area cushion-like saTENG touched by human skin.

movie S7. Harvesting mechanical energy based on household plumbing using flowing water as the electrode.

movie S8. Harvesting energy from arm swing by a saTENG working in the single-electrode sliding mode.

movie S9. Harvesting energy from arm motion by an attached-electrode-mode saTENG.

movie S10. Harvesting energy from moving a mouse by a freestanding-mode saTENG.

movie S11. Harvesting energy from human walking by a freestanding-mode saTENG.